

Structure study of a dielectric laser accelerator with discrete translational symmetry

Yangfan He(何阳帆), Bin Sun(孙斌), Mingjiang Ma(马铭江), Wei Li(李伟), Zhihao Cui(崔志浩), and Zongqing Zhao(赵宗清)

Citation: Chin. Phys. B, 2023, 32 (**11**): 114101. DOI: 10.1088/1674-1056/acc05a
Journal homepage: http://cpb.iphy.ac.cn; http://iopscience.iop.org/cpb

What follows is a list of articles you may be interested in

Structure and material study of dielectric laser accelerators based on the inverse Cherenkov effect

Bin Sun(孙斌), Yang-Fan He(何阳帆), Ruo-Yun Luo(罗若云), Tai-Yang Zhang(章太阳), Qiang Zhou(周强), Shao-Yi Wang(王少义), Du Wang(王度), and Zong-Qing Zhao(赵宗清)
Chin. Phys. B, 2023, 32 (**9**): 094101. DOI: 10.1088/1674-1056/acdc0a

Particle-in-cell simulations of low-β magnetic reconnection driven by laser interaction with a capacitor-coil target

Xiaoxia Yuan(原晓霞), Cangtao Zhou(周沧涛), Hua Zhang(张华), Ran Li(李然), Yongli Ping(平永利), and Jiayong Zhong(仲佳勇)
Chin. Phys. B, 2023, 32 (**5**): 054101. DOI: 10.1088/1674-1056/acb911

Plasma density transition-based electron injection in laser wake field acceleration driven by a flying focus laser

Pan-Fei Geng(耿盼飞), Min Chen(陈民), Xiang-Yan An(安相炎), Wei-Yuan Liu(刘维媛), Xin-Zhe Zhu(祝昕哲), Jian-Long Li(李建龙), Bo-Yuan Li(李博原), and Zheng-Ming Sheng(盛政明)
Chin. Phys. B, 2023, 32 (**4**): 044101. DOI: 10.1088/1674-1056/acae79

Generation of laser-driven flyer dominated by shock-induced shear bands: A molecular dynamics simulation study

Deshen Geng(耿德珅), Danyang Liu(刘丹阳), Jianying Lu(鲁建英), Chao Chen(陈超), Junying Wu(伍俊英), Shuzhou Li(李述周), and Lang Chen(陈朗)
Chin. Phys. B, 2022, 31 (**2**): 024101. DOI: 10.1088/1674-1056/ac2f2d

Terahertz radiation generation by beating of two chirped laser pulses in a warm collisional magnetized plasma

Motahareh Arefnia, Mehdi Sharifian, and Mohammad Ghorbanalilu
Chin. Phys. B, 2021, 30 (**9**): 094101. DOI: 10.1088/1674-1056/abfb5d

---

Structure study of a dielectric laser accelerator with discrete translational symmetry

Yangfan He(何阳帆)[1,2,†], Bin Sun(孙斌)[1,2,3], Mingjiang Ma(马铭江)[4], Wei Li(李伟)[1,2], Zhihao Cui(崔志浩)[1,2], and Zongqing Zhao(赵宗清)[1,‡]

[1] *Laser Fusion Research Center, CAEP, Mianyang* 621900, *China*
[2] *The Sciences and Technology on Plasma Physics Laboratory, CAEP, Mianyang* 621900, *China*
[3] *University of Science and Technology of China, Hefei* 230026, *China*
[4] *The Institute of Optics, University of Rochester, Rochester, NY* 14627, *USA*

(Received 21 November 2022; revised manuscript received 16 February 2023; accepted manuscript online 2 March 2023)

The dielectric laser accelerator (DLA) is a promising technology for achieving high-gradient acceleration in a compact design. Its advantages include ease of cascading and an energy gain per unit distance which can exceed that of conventional accelerators by two orders of magnitude. This paper establishes rules for efficient particle acceleration using dielectric structures based on basic equations, proposes a design principle for DLA structures with clear physical images and verifies the accuracy of the corresponding formula for energy gain. DLA structures with different specifications, materials and geometric shapes are constructed, and the achievable acceleration gradient is calculated. Our results demonstrate that effective acceleration can be achieved when the electric field sensed by particles in the acceleration cavity has zero frequency, which provides a powerful method for designing such devices. Furthermore, we demonstrate that the simplified formula for calculating energy gain presented in this paper can accurately determine the energy gain of particles during the design of acceleration structures using a dielectric accelerator.

Keywords: dielectric laser accelerator, acceleration structure, high-gradient accelerator

PACS: 41.75.Jv, 41.20.Jb, 42.25.–p, 41.20.–q **DOI:** 10.1088/1674-1056/acc05a

1. Introduction

Particle accelerators play a crucial role in fundamental science, as well as in various practical applications such as cancer treatment, materials analysis and food and water purification.[1–4] Traditional accelerators use radio-frequency klystrons to excite modes in copper or superconducting niobium cavities for particle acceleration, but their large size, high power requirements and expensive infrastructure limit their accessibility to the broader scientific community. This has promoted the exploration of more compact and economical alternative technologies.

With the advancement of microfabrication and laser technology, many ideas have been practically implemented, such as the use of terahertz interaction with microstructures to accelerate charged particles,[5] ultra-intense ultrafast lasers to interact with plasma for particle acceleration[6,7] and high fields in ultrafast pulsed laser beams to accelerate electron beams in dielectric microstructures.[8] In general, the acceleration gradient determines the total length of the accelerator at a specific beam energy. Therefore, in the process of developing advanced compact accelerators, acceleration techniques should achieve high energy gain per unit length. Recently, dielectric laser accelerators (DLAs) have attracted significant interest as a means of accelerating charged particles using solid-state lasers.[9–16] In various experiments, an acceleration gradient of nearly 1 GV·m^{-1} has been achieved (see Ref. [17] and the references therein). DLAs are promising candidates for realizing future compact and low-cost particle accelerators due to their high energy gain per unit length, which is second only to that of laser-plasma accelerators.[18–24] In addition, DLAs have the advantage of easy integration of cascade acceleration.[25–27]

The design of effective micro/nano dielectric structures to generate accelerating fields driven by input lasers is a critical research topic for DLAs. There are various explanations for the acceleration principle of DLAs, including the phase modulation principle proposed by Plettner *et al.*,[28] and the analysis of accelerating field mode by Breuer *et al.*[29] for single and double gratings. Aimidula *et al.*[30] found that an asymmetric double grating structure can synchronize the laser field with relativistic electrons. Niedermayer *et al.*[31] used a Fourier transform and the Panofsky–Wenzel theorem to model grating accelerators. Kozák *et al.*[32] studied the interaction between evanescent waves and electrons using classical approximation, while Liu *et al.*[33] studied the field distribution in the accelerating cavity using classical electrodynamics. A comprehensive theory of the Lorentz force in a double grating medium laser accelerator was proposed by Black *et al.*[34] The phase modulation principle proposed in these references is commonly used in the design of DLAs (see Ref. [28] and citations therein). It is worth noting that the phase modulation

†Corresponding author. E-mail: heyangfan@mail.ustc.edu.cn
‡Corresponding author. E-mail: zhaozongqing99@caep.ac.cn
© 2023 Chinese Physical Society and IOP Publishing Ltd

principle used in the design of DLAs is based on geometrical optics. The concept that DLA achieves acceleration when the particle experiences a zero-frequency electric field inspired this study. The physical analogy can be likened to a particle riding a fixed-phase acceleration in the accelerating field.

In this study, we have developed rules for efficient particle acceleration using dielectric structures based on the fundamental equations of electromagnetism. This paper is organized as follows. In Section 2, we elaborate on the rules for efficient particle acceleration with dielectric structures using basic equations. In Section 3, we show the modeling process of the dielectric accelerator in the finite-difference frequency domain (FDFD) in detail. In Section 4, we validate the simplified formula for calculating energy gain, design DLA structures with different parameters and calculate the acceleration gradient using three different materials.

2. Structures and principles

Our starting point, naturally, is Maxwell's equations in SI units[35]

$$\begin{aligned}
&\nabla\cdot\varepsilon\boldsymbol{E}=\rho,\\
&\nabla\times\boldsymbol{E}=-\frac{\partial\mu\boldsymbol{H}}{\partial t},\\
&\nabla\cdot\mu\boldsymbol{H}=0,\\
&\nabla\times\boldsymbol{H}=\boldsymbol{J}+\frac{\partial\varepsilon\boldsymbol{E}}{\partial t},
\end{aligned}\tag{1}$$

where $\boldsymbol{E}$ is electric field, ρ is the free charge density, $\boldsymbol{H}$ is the magnetic field, $\boldsymbol{J}$ is the free current density, μ is the permeability of the material and ε is the dielectric function. All of these are potentially functions of both the position $\boldsymbol{r}$ and the time t. In this paper, we work with non-magnetic materials, $\mu=\mu_0$ (permeability of free space). The input energy for acceleration is achieved by applying an electric field. We assume the electron is suitably 'beam-like' such that $\beta_x\approx\beta=v/c$, where v is the velocity of the particle. So, the rate of change of energy can be described by

$$\partial_x\gamma=qE_x^{\mathrm{p}}/m_{\mathrm{p}}c^2,\tag{2}$$

where q is the charge of the particle, γ is the Lorentz factor, $m_{\mathrm{p}}c^2$ is the rest mass of the particle and E_x^{p} here is the electric field felt by the particles.

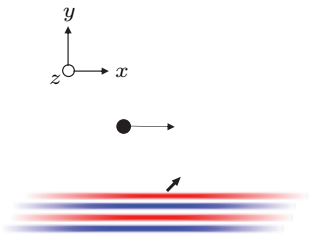


Fig. 1. The charged particles in a vacuum interact with the plane wave. In this study, we consider a vacuum as a medium with continuous translational symmetry.

The mathematical form of E_x^{p} can be artificially designed to be very complex. Fortunately, mathematical theorems guarantee that any electromagnetic field can be decomposed into a superposition of several sine waves via the Fourier transform. This is physically equivalent to the interaction between a plane wave and an electron in a vacuum. In free space, as shown in Fig. 1, E_x^{p} is an oscillating electromagnetic field

$$E_x^{\mathrm{p}}=E_0\cos(\omega t+kz_{\mathrm{p}}+\delta),\tag{3}$$

where δ is the initial phase of particle injection, E_0 is a constant, ω is the frequency of the incident light, k is the wavevector (here $k=2\pi/\lambda$, where λ is the wavelength of the incident light). In a period, it can be assumed that the particles move along a straight line, $z_{\mathrm{p}}=z_0$ in Eq. (3), where z_0 is the initial injection point of the particle in the z-direction. It can be seen that the rate of change of energy of the particle increases and decreases alternately at the frequency ω by combining Eqs. (2) and (3). In other words, the net energy gain of the interaction between a charged particle and an oscillating electromagnetic field is zero, because the odd trigonometric function with time-dependent terms in the expression for electric field experienced by the particle (such as E_x^{p} in Eq. (3)) is zero on average over a period. Therefore, to achieve acceleration without dephasing, the odd-order trigonometric function should have no time term or not depend on x. To achieve effective acceleration means that particles (from their reference frame) experience a "zero-frequency" electric field.

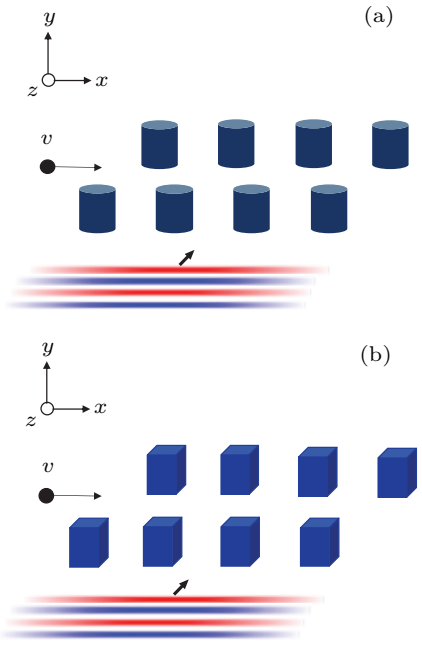


Fig. 2. (a) The cylindrical medium is arranged periodically in the x-direction. (b) The cuboid medium is arranged periodically in the x-direction. It should be noted that the laser can also be incident in the y-direction. The theoretical description in this paper is equally applicable to this situation. The only difference is that a three-dimensional simulation is required.

We note that in the expression describing the electric field experienced by the particle, t should be treated as an implicit function of the path length along the accelerator (x). This treatment revealed a very natural way to construct the "zero-frequency" electric field felt by particles, which is to use some kind of structure to break the translational symmetry of free space, as shown in Fig. 2,

$$\boldsymbol{\epsilon}(\boldsymbol{x}+\boldsymbol{T})=\boldsymbol{\epsilon}(\boldsymbol{x}),\quad \boldsymbol{x}\in R^3,\quad \boldsymbol{T}\in L, \tag{4}$$

where $L=\{\boldsymbol{T}=N_1\boldsymbol{a}_1+N_2\boldsymbol{a}_2+N_3\boldsymbol{a}_3|N_1,N_2,N_3\in Z\}$; let $\boldsymbol{a}_1,\boldsymbol{a}_2$ and $\boldsymbol{a}_3$ be the linearly independent and non-vanishing vectors of R^3 defining the unit cell of the periodic structure. Due to the translational symmetry, the Floquet–Bloch theorem[36,37] implies

$$\boldsymbol{E}(\boldsymbol{r})=\boldsymbol{E}_{\boldsymbol{k}}(\boldsymbol{r})\,\mathrm{e}^{\mathrm{i}\boldsymbol{k}^{\mathrm{Bloch}}\cdot\boldsymbol{r}},\quad \boldsymbol{E}_{\boldsymbol{k}}(\boldsymbol{r}+\boldsymbol{T})=\boldsymbol{E}_{\boldsymbol{k}}(\boldsymbol{r}), \tag{5}$$

where $\boldsymbol{k}^{\mathrm{Bloch}}$ is the Bloch wavevector. Due to the periodicity of $\boldsymbol{E}_{\boldsymbol{k}}(\boldsymbol{r})$, we can express the spatial fields in terms of the Fourier series

$$\boldsymbol{E}(\boldsymbol{r})=\sum_{\boldsymbol{G}}\boldsymbol{E}_{\boldsymbol{k}}(\boldsymbol{G})\,\mathrm{e}^{\mathrm{i}(\boldsymbol{k}^{\mathrm{Bloch}}+\boldsymbol{G})\cdot\boldsymbol{r}}, \tag{6}$$

where $\boldsymbol{G}$ is the inverse lattice vector of the reciprocal space. Without loss of generality, discrete periodicity is introduced in the direction of particle motion ($\boldsymbol{T}=\Lambda\boldsymbol{e}_{\boldsymbol{x}}$). Because the fundamental features of DLA appear in the simplified 2D analysis, the full-field variation with z is not considered for the time being. This means $\partial\boldsymbol{E}/\partial z=0$ and $\partial\boldsymbol{H}/\partial z=0$. We apply Eq. (6) to obtain

$$E_x(x,y)=\mathcal{R}\left\{\sum_{N=-\infty}^{N=\infty}E_N(y)\,\mathrm{e}^{\mathrm{i}k_\Lambda^* x}\mathrm{e}^{-\mathrm{i}\omega t}\right\}, \tag{7}$$

where $k_\Lambda^*=k_\Lambda^N+k_x^{\mathrm{Bloch}}$, $k_\Lambda^N=2\pi N/\Lambda$, $\omega=2\pi c/\lambda$ and $E_x(x,y)$ is the longitudinal electric laser field in the DLA cell (Λ). $E_N(y)$ is the nth-order Fourier coefficient

$$E_N(y)=\frac{1}{\Lambda}\int_0^{\Lambda}\boldsymbol{E}_k(x,y)\,\mathrm{e}^{-\mathrm{i}k_\Lambda^N x}\mathrm{d}x. \tag{8}$$

To calculate the motion of electrons in a short DLA, it is usually safe to assume that the electrons are very rigid, so they do not deviate from the trajectory they were on before the DLA. In Eq. (7), t should be seen as an implicit function of the path length $x=vt-l$ along the accelerator. The phase shift between laser phase and particle injection phase is described by the distance l. We can obtain an expression for the electric field felt by the particle

$$E_x^{\mathrm{p}}=\mathcal{R}\left\{\mathrm{e}^{-\mathrm{i}k_\Lambda^* l}\sum_{N=-\infty}^{N=\infty}E_N(y)\,\mathrm{e}^{\mathrm{i}c(k_\Lambda^*\beta-k_0)t}\right\}, \tag{9}$$

where $k_0=\omega/c$. The first-order trigonometric function of the time term is eliminated from equation Eq. (9), which means that there is a constraint

$$k_\Lambda^*=k_0/\beta. \tag{10}$$

In other words, after the constraint $k_\Lambda^*=k_0/\beta$ is imposed on a structure with discrete translational symmetry, the particles are sensed by an electric field of zero frequency. k_Λ^* depends on the particle velocity at the time of injection into the structure. This means that for long-range acceleration of non-relativistic particles, the parameters k_Λ^* need to be adjusted in real time. Injection of ultra-relativistic particles does not require adjustment of parameters k_Λ^* during long-range acceleration. Equation (10) is also called the synchronization condition in the accelerator.[8] The energy gain in a period is simplified as

$$\Delta W_x(l,y)=q\Lambda\mathcal{R}\left\{E_N(y)\,\mathrm{e}^{\mathrm{i}\omega l/v}\right\}. \tag{11}$$

This equation is hereinafter referred to as the simplified energy formula. The summation operation disappears here. This means that the energy gain of the particle is proportional to the nth-order Fourier coefficient.

3. Methods

To meet the requirements of low memory usage and computational time, we employed the FDFD method to solve for the field distribution of the structure at a given frequency (ω) in a DLA coupled with non-magnetic materials under typical conditions. We assume that all the fields have the $\mathrm{e}^{-\mathrm{i}\omega t}$ dependence with ω being the angular frequency ($\boldsymbol{E}(\boldsymbol{r},t)=\mathcal{R}\{\boldsymbol{E}(\boldsymbol{r})\mathrm{e}^{-\mathrm{i}\omega t}\}$, $\boldsymbol{H}(\boldsymbol{r},t)=\mathcal{R}\{\boldsymbol{H}(\boldsymbol{r})\mathrm{e}^{-\mathrm{i}\omega t}\}$). The electromagnetic distribution of the system can be calculated from

$$\begin{aligned}&(\nabla_x^E\varepsilon^{-1}\nabla_x^H+\nabla_y^E\varepsilon^{-1}\nabla_y^H+\omega^2/c^2)H_z=\mathrm{i}\omega J_z,\\&\nabla_y^H H_z=\mathrm{i}\omega\varepsilon_0\varepsilon E_x,\quad \nabla_x^H H_z=\mathrm{i}\omega\varepsilon_0\varepsilon E_y.\end{aligned} \tag{12}$$

Here ε is the dielectric function. The terms ∇_x^E and ∇_y^E are banded matrices that calculate the first-order spatial derivatives of the electric fields across the grid. The derivative operators for the electric and magnetic fields are different due to the staggered nature of the Yee grid,[38] but they are related through

$$\nabla_x^H=-(\nabla_x^E)^{\mathrm{HT}},\quad \nabla_y^H=-(\nabla_y^E)^{\mathrm{HT}}. \tag{13}$$

The "HT" superscript indicates a Hermitian transpose operation.[39] TE mode should be used to produce particle acceleration. Here we apply the sparse matrix technique to save computation time and memory. As a quick example of what these matrices look like, they were computed for a two-dimensional grid composed of only 3×3 cells. Using periodic boundaries conditions, the matrix derivative operators ∇_x^E and ∇_y^E for the simple case are

$$\nabla_x^E = \frac{1}{\Delta y}\begin{bmatrix} -1 & 1 & & & & & & & \\ & -1 & 1 & & & & & & \\ U_x & & -1 & 0 & & & & & \\ & & & -1 & 1 & & & & \\ & & & & -1 & 1 & & & \\ & & & U_x & & -1 & 0 & & \\ & & & & & & -1 & 1 & \\ & & & & & & & -1 & 1 \\ & & & & & & U_x & & -1 \end{bmatrix}, \quad (14)$$

$$\nabla_y^E = \frac{1}{\Delta x}\begin{bmatrix} -1 & & & 1 & & & & & \\ & -1 & & & 1 & & & & \\ & & -1 & & & 1 & & & \\ & & & -1 & & & 1 & & \\ & & & & -1 & & & 1 & \\ V_y & & & & & -1 & & & \\ & V_y & & & & & -1 & & \\ & & V_y & & & & & -1 & \end{bmatrix}, \quad (15)$$

where $\Delta x\,(\Delta y)$ is the FDFD Yee grid size along the $x\,(y)$-direction, $U_x = \mathrm{e}^{\mathrm{i}k_x^{\mathrm{Bloch}}}$, $V_y = \mathrm{e}^{\mathrm{i}k_y^{\mathrm{Bloch}}}$ and $k_{x(y)}^{\mathrm{Bloch}}$ is the phase across a periodic boundary in $x\,(y)$. Similarly, the terms ∇_x^H and ∇_y^H calculate the first-order spatial derivatives of the magnetic fields across the grid. To ensure accurate simulation results, it is crucial to choose a grid spacing that is small enough to resolve the shortest wavelength of interest. This is usually determined as $\lambda_{\min}/10$ to $\lambda_{\min}/30$, where $\lambda_{\min}/10$ represents the shortest wavelength in the region with the highest refractive index. In this simulation, a square grid size (Δx (Δy)) of approximately $\lambda/100$ can be selected based on previous studies.[40,41] To simplify matters, this paper does not directly verify the energy gain but instead focuses on the normalized acceleration gradient function G_{nor} derived from it. There are two methods for calculating it: (a) The direct integration method is used to calculate the normalized acceleration gradient function, G_{nor}, in the periodic structure,

$$G_{\mathrm{nor}} \equiv \frac{1}{\Lambda E_0}\int_0^{\Lambda} E_x\left(x, y; t = \frac{x}{\beta c}\right)\mathrm{d}x. \quad (16)$$

(b) The normalized acceleration gradient function, G_{nor}, calculated using the simplified energy formula (Eq. (11) can be represented by

$$G_{\mathrm{nor}} \equiv \frac{\Delta W_x}{q\Lambda E_0} = \frac{\mathcal{R}\left\{E_N(y)\,\mathrm{e}^{\mathrm{i}\omega l/v}\right\}}{E_0}. \quad (17)$$

4. Results

4.1. Parameter optimization

The DLA structure parameters are shown in Fig. 3(a), where H is the height of the medium, D is the width of the medium, Λ is the period length of the structure and A is the width of the acceleration channel. All length units are normalized by the incident wavelength. Since the accelerating electric field mode is an evanescent wave, increasing the value of A will decrease the amplitude of the accelerating mode. However, if A is too small, it may cause difficulties in the electron injection process. Therefore, a compromise is to choose $A(\lambda)$ as $1/4$. In this study, we only consider the periodic structure with more symmetry, which means D is equal to $\beta/2$, as shown in Table 1.

Table 1. The parameters used in the simulation. All length units are normalized by the incident wavelength.

λ	SiO_2	Si_3N_4	Si	$\Lambda(\lambda)$	$A(\lambda)$	$D(\lambda)$
2000 nm	$\varepsilon = 2.1$	$\varepsilon = 3.9$	$\varepsilon = 11.8$	β	1/4	$\beta/2$

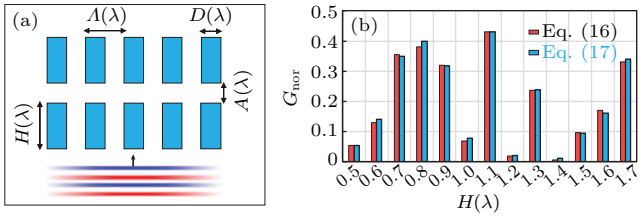


Fig. 3. (a) DLA structure parameters. Only $H(\lambda)$ is varied in the simulation. (b) Acceleration gradient for different parameters $H(\lambda)$.

The region of the particle injection channel is of size $4\lambda \times \lambda/4$, $\beta = 0.8$, the pillar size is $H(\lambda) \times 0.4\lambda$. A periodic condition is used to introduce plane waves into the structure from the lower side, as shown in Fig. 3(a). For materials of Si, we calculated the value of G_{nor} on the symmetry line of the particle injection channel by using Eqs. (16) and (17). A total of 13 parameter simulations were performed, where only $H(\lambda)$ was varied, as shown in Fig. 3(b). G_{nor} reaches a peak of 0.43 for $H(\lambda) = 1.1$. In other words, when the structure parameter of the Si pillar is 2200 nm × 800 nm, an acceleration gradient of 0.43 times the initial electric field value can be provided at the center of the particle channel, which corresponds to an acceleration gradient of 0.12 GV·m^{-1} calculated based on Refs. [40,41]. It is evident that for the majority of cases, the results obtained from Eqs. (16) and (17) are extremely close, with only slight differences in a few instances. Additionally, we observe that as the value of H increases, the calculated results also increase or decrease. However, this trend is not strictly linear, and at times there may be small fluctuations. Therefore, the design of the accelerator needs to be analyzed on a case-by-case basis at a machinable scale.

4.2. Influence of electrons

We simulate the acceleration of different electrons using the optimal H obtained from the previous simulation and analyze their impact on the acceleration. A periodic condition is used to introduce plane waves into the structure from the lower side. The region of the particle injection channel is of size $5\beta\lambda \times \lambda/4$, The pillar size is $\beta\lambda/2 \times 1.1\lambda$. A total of seven simulations were performed, where only β was varied. We calculated the value of G_{nor} on the symmetry line of the particle injection channel. The results of these two methods are shown in Fig. 4(a).

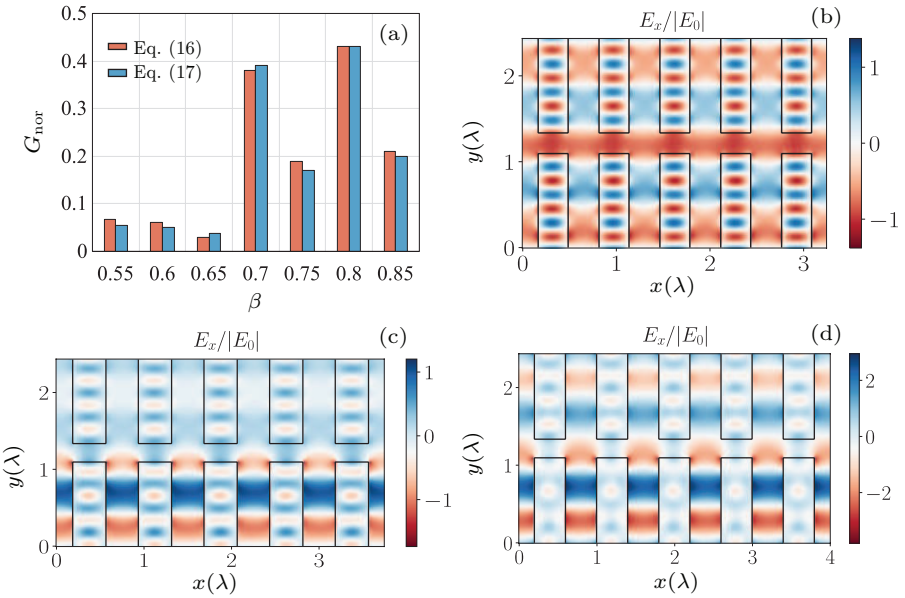


Fig. 4. Values of electric field distribution and normalized acceleration gradient function. (a) The values of the normalized acceleration gradient function calculated by two different methods, Eqs. (16) and (17), with seven β parameters. The electric field distributions shown in (b), (c) and (d) correspond to the simulation parameters β of 0.65, 0.75 and 0.8, respectively.

The relationship between β and $G_{\rm nor}$ is not linear but exhibits a complex nonlinear relationship. When β varies between 0.55 and 0.6, the value of $G_{\rm nor}$ decreases slightly; when β varies between 0.6 and 0.65, the value of $G_{\rm nor}$ decreases more significantly; when β varies between 0.65 and 0.7, the value of $G_{\rm nor}$ drops sharply, but then rapidly rebounds after 0.7; when β varies between 0.7 and 0.8, the value of $G_{\rm nor}$ fluctuates widely but shows an overall upward trend; and when β varies between 0.8 and 0.85, the value of $G_{\rm nor}$ decreases slightly but still remains at a high level. The general trend is that as β increases, the value of $G_{\rm nor}$ first increases and then decreases. It can be seen that the $G_{\rm nor}$ values obtained by the two calculation methods are in good agreement.

We have plotted the electric field distributions in Figs. 4(b), 4(c) and 4(d) for beta values of 0.65, 0.75 and 0.8, respectively. It is evident that the main difference between the beta values of 0.65 and 0.75/0.8 lies in the mode pattern of the electric field distribution, with the standing wave mode in the latter case being more conducive to electron acceleration. Analyzing the electric field distribution between beta values of 0.75 and 0.8, it can be observed that although standing wave modes can be excited in both cases, the strength of the excitation is different. A stronger standing wave mode is excited for a beta value of 0.8, which results in a stronger corresponding acceleration gradient.

Using Eqs. (16) and (17), we have calculated 20 different examples. These results indicate that neglecting the charge space effect during acceleration over a short distance results in highly accurate calculations of the maximum acceleration gradient using the simplified energy formula. However, it is expected that the deflection field will affect the accuracy of calculation of the maximum acceleration gradient during acceleration over a long distance, although the formula for energy gain of particles in the longitudinal direction remains valid.

4.3. Influence of material

Based on the optimal layout obtained from the previous simulation, we conducted simulations using three available materials and analyzed how the electric field distribution affects the acceleration.

The region of the particle injection channel is of size $4\lambda \times \lambda/4$ and $\beta = 0.8$. A periodic condition is used to introduce plane waves into the structure from the lower side, as shown in Fig. 3(a). A total of three simulations were performed, where only the ε parameter was varied. We calculated the value of $G_{\rm nor}$ on the symmetry line of the particle injection channel. For the materials SiO_2, Si_3N_4 and Si, the acceleration gradients achieved were 0.01, 0.08 and 0.43 (E_0), respectively. Assuming incident field values consistent with the laser damage thresholds given in references,[40,41] these correspond to acceleration gradients of 0.003 GV·m^{-1}, 0.11 GV·m^{-1} and 1.8 GV·m^{-1}, respectively.

In Figs. 5(a), 5(b) and 5(c), we depict the electric field distributions corresponding to SiO_2, Si_3N_4 and Si, respectively. It is evident that the primary difference among the three materials lies in the mode of electric field distribution. Specifically, the standing wave mode in Si is more conducive to electron acceleration. Si can excite a stronger standing wave mode, resulting in a stronger corresponding acceleration gradient. Therefore, this implies that the greater the refractive index contrast in the structure, the more suitable it is for particle acceleration. Therefore, this result once again confirms that a case-by-case analysis is required in the design process of the accelerator.

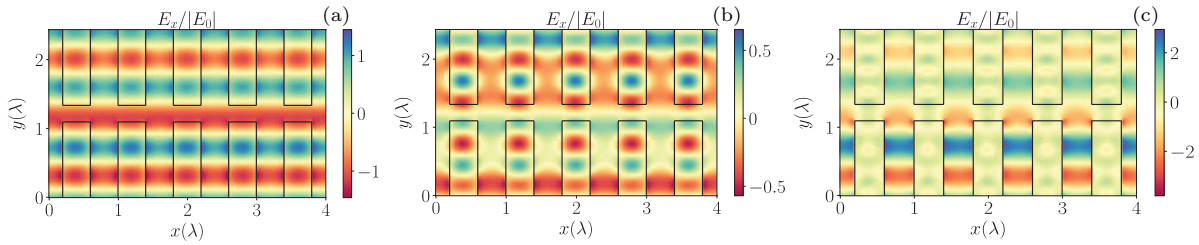


Fig. 5. Electric field distributions of cylindrical structures with three different materials: (a) SiO_2, (b) Si_3N_4 and (c) Si.

5. Conclusion

In this study, we establish the principles for effectively accelerating particles using dielectric structures by using basic equations, and provide a clear understanding of the physical mechanism behind acceleration by DLAs. We demonstrate how DLAs can be implemented by breaking spatial symmetry and validate our calculations using the FDFD method, which supports the use of simplified energy formulae to compute particle energy gain in large-scale simulations. We also demonstrate that effective acceleration occurs when particles in the acceleration cavity sense an electric field with zero frequency, which offers a powerful method for designing these devices. Overall, our results provide a new physical framework for understanding the mechanism of acceleration by a DLA, and have potential applications in the field of designing dielectric laser acceleration.

Acknowledgements

The authors are grateful to Fulong Liu and Qiangyou He for fruitful discussions.

Project supported by the National Natural Science Foundation of China (Grant No. 11975214).

References

[1] McNeil B W and Thompson N R 2010 *Nat. Photonics* **4** 814
[2] Bulanov S V and Khoroshkov V S 2002 *Plasma. Phys. Rep.* **28** 453
[3] Ginzton E L, Hansen W W and Kennedy W R 1948 *Rev. Sci. Instrum.* **19** 89
[4] Schardt D, Elsässer T and Ertner D S 2010 *Rev. Sci. Instrum.* **82** 383
[5] Nanni E A, Huang W R, Hong K H, Ravi K, Fallahi A, Moriena G, Miller R J and Kärtner F X 2015 *Nat. Commun.* **6** 8486
[6] Esarey E, Schroeder C B and Leemans W P 2009 *Rev. Mod. Phys.* **81** 1229
[7] Macchi A, Borghesi M and PassoniIon M 2013 *Rev. Mod. Phys.* **85** 751
[8] England R J, Noble R J, Bane K, Dowell D H, Ng C K, Spencer J E, Tantawi S, Wu Z, Byer R L, Peralta E and Soong K 2014 *Rev. Mod. Phys.* **86** 1337
[9] Breuer J and Hommelhoff P 2013 *Phys. Rev. Lett.* **111** 134803
[10] Peralta E A, Soong K, England R J, Colby E R, Wu Z, Montazeri B, McGuinness C, McNeur J, Leedle K J, Walz D, Sozer E B, Cowan B, Schwartz B, Travish G and Byer R L 2013 *Nature* **503** 91
[11] Leedle K J, Pease R F, Byer R L and Harris J S 2015 *Optica* **2** 158
[12] Leedle K J, Ceballos A, Deng H Y, Solgaard O, Pease R F, Byer R L and Harris J S 2015 *Opt. Lett.* **40** 4344
[13] Niedermayer U, Egenolf T, Boine-Frankenheim O and Hommelhoff P 2018 *Phys. Rev. Lett.* **121** 21480
[14] Black D S, Leedle K J, Miao Y, Niedermayer U, Byer R L and Solgaard O (ACHIP Collaboration) 2019 *Phys. Rev. Lett.* **122** 104801
[15] Schönenberger N, Mittelbach A, Yousefi P, McNeur J, Niedermayer U and Hommelhoff P 2019 *Phys. Rev. Lett.* **123** 264803
[16] Black D S, Niedermayer U, Miao Y, Zhao Z X, Solgaard O, Byer R L and Leedle K J 2019 *Phys. Rev. Lett.* **123** 264802
[17] Wootton K P, McNeur J and Leedle K J 2016 *Rev. Accelerator Sci. Technol.* **9** 105
[18] Faure J, Glinec. Y, Pukhov A, Kiselev S, Gordienko S, Lefebvre E, Rousseau J P, Burgy F and Malka V 2004 *Nature* **431** 541
[19] Leemans W P, Nagler B, Gonsalves A J, Tóth Cs, Nakamura K, Geddes C G R, Esarey E, Schroeder C B and Hooker S M 2006 *Nat. Phys.* **2** 696
[20] Esarey E, Schroeder C B and Leemans W P 2009 *Rev. Mod. Phys.* **81** 1229
[21] Corde S, Ta Phuoc K, Lambert G, Fitour R, Malka V, Rousse A, Beck A and Lefebvre E 2013 *Rev. Mod. Phys.* **85** 1
[22] Hong X R, Zhou W J, Xie B S, Yang Y, Wang L, Tian J M, Tang R A and Duan W S 2017 *Chin. Phys. B* **26** 65203
[23] Yue D N, Chen M, Zhao Y, Geng P F, Yuan X H, Dong Q L, Sheng Z M and Zhang J 2022 *Chin. Phys. B* **31** 045205
[24] Zhang Q, Ping Y L, An W M, Sun W and Zhong J Y 2022 *Chin. Phys. B* **31** 065203
[25] Hughes T, Tan S, Zhao Z X, Sapra N V, Leedle K J, Deng H Y, Miao Y, Black D S, Solgaard O, Harris J S, Vuckovic J, Byer R L, Fan S H, England R J, Lee Y J and Qi M H 2018 *Phys. Rev. Appl.* **9** 054017
[26] Sapra N V, Yang K Y, Vercruysse D, Leedle K J, Black D S, England R J, Su L, Trivedi R, Miao Y, Solgaard O, Byer R L and Vuckovic J 2020 *Science* **367** 79
[27] Niedermayer U, Lautenschläger J, Egenolf T and Boine-Frankenheim O 2021 *Phys. Rev. Appl.* **16** 024022
[28] Plettner T, Lu P P and Byer R L 2006 *Phys. Rev. Spec. Top. Accel Beams* **9** 111301
[29] Breuer J, McNeur J and Hommelhoff P 2014 *J. Phys. B: At. Mol. Opt. Phys.* **47** 234004
[30] Aimidula A, Bake M A, Wan F, Xie B S, Welsch C P, Xia G, Mete O, Uesaka M, Matsumura Y, Yoshida M and Koyama K 2014 *Phys. Plasmas* **21**023110
[31] Niedermayer U, Egenolf T and Boine-Frankenheim O 2017 *Phys. Rev. Accel. Beams* **20** 111302
[32] Kozák M, Beck P, Deng H, McNeur J, Schönenberger N, Gaida C, Stutzki F, Gebhardt M, Limpert J, Ruehl A, Hartl I, Solgaard O, Harris J S, Byer R L and Hommelhoff P 2017 *Opt. Express* **25** 19195
[33] Liu W H, Yu Z, Sun L, Liu Y C, Jia Q K, Xu H and Sun B G 2020 *Phys. Rev. Appl.* **14** 014018
[34] Black D S, Zhao Z X, Leedle K J, Miao Y, Byer R L, Fan S H and Solgaard O 2020 *Phys. Rev. Accel. Beams* **23** 114001
[35] Maxwell J C 1865 *Phil. Trans. R. Soc. London* **155** 459
[36] Bloch F 1929 *Z. Phys.* **52** 555
[37] Floquet G 1883 *Ann. Sci. Ecole Norm. S* **12** 47
[38] Yee K 1966 *IEEE. Trans. Antennas Propag.* **14** 302
[39] Rumpf R C 2012 *Prog. Electromagn. Res. B* **36** 221
[40] He Y F, Sun B, Ma M J , Li W, He Q Y, Cui Z H, Wang S Y and Zhao Z Q 2022 *Nucl. Sci. Tech.* **33** 120
[41] Hughes T, Veronis G, Wootton K P, England R J and Fan S H 2017 *Opt. Express* **25** 15414